ENGINEERING

Programmable allosteric DNA regulations for molecular networks and nanomachines

Cheng Zhang[1]*†, Xueying Ma[2,3]†, Xuedong Zheng[4]†, Yonggang Ke[5,6], Kuiting Chen[2], Dongsheng Liu[7], Zuhong Lu[8], Jing Yang[2]*, Hao Yan[9,10]*

Structure-based molecular regulations have been widely adopted to modulate protein networks in cells and recently developed to control allosteric DNA operations in vitro. However, current examples of programmable allosteric signal transmission through integrated DNA networks are stringently constrained by specific design requirements. Developing a new, more general, and programmable scheme for establishing allosteric DNA networks remains challenging. Here, we developed a general strategy for programmable allosteric DNA regulations that can be finely tuned by varying the dimensions, positions, and number of conformational signals. By programming the allosteric signals, we realized fan-out/fan-in DNA gates and multiple-layer DNA cascading networks, as well as expanding the approach to long-range allosteric signal transmission through tunable DNA origami nanomachines ~100 nm in size. This strategy will enable programmable and complex allosteric DNA networks and nanodevices for nanoengineering, chemical, and biomedical applications displaying sense-compute-actuate molecular functionalities.

INTRODUCTION

Biological systems use biochemical networks to execute signal transductions and regulate biofunctions (*1*–*3*). Cellular messages are delivered to targets by coordinating and concatenating multiple networks (*4*–*6*). Biomolecular networks process various chemical or physical signals, including chemical bonds, intermolecular forces, and conformational changes, to constitute complex biochemical pathways (*5*, *7*–*10*). In particular, structure-based molecular signaling has evolved to regulate a wide range of molecular pathways in cells (*11*–*14*). For example, allosteric signals are typically organized and engineered into programmable networks to regulate protein receptors (*15*–*18*).

In biosystems, molecular programmability involves the assembly of individual building blocks into hierarchical biochemical networks that play important roles in information processing (*19*–*23*). The high programmability of DNA complementarity is particularly suitable for designing complex synthetic DNA systems (*24*–*29*). Many DNA regulation strategies have been developed for engineering programmable DNA networks, such as toehold mediation, aptamer initiation, light or pH control, electric field driven, and enzyme assisted (*30*–*37*). Recently, the strand displacement reaction (SDR) has been developed as a powerful regulation tool for programmable DNA operations and SDR has been exploited to engineer complex cascades and hierarchical DNA networks (*38*–*40*). The programmable-design SDRs between input/output (I/O) DNA strands facilitate systematic molecular information transfer and signal transduction within DNA networks (*41*–*43*).

Because DNA secondary structures can be governed precisely by programming base pairing, it is desirable to design specific conformational signals to regulate DNA operations (*44*–*46*). Recent efforts to allosterically control synthetic DNA systems have been constructed by mimicking allosteric signal modulations, as found in protein receptors (*47*–*50*). However, current programmable allosteric DNA regulations (PADRs) are stringently constrained because of the difficulties in cascading conformation designs, such as integration, tunability, and transmissibility during the multiple allosteric signal transductions. Therefore, developing a new, more general, and PADR scheme to engineer complex conformational signal pathways remains a substantial challenge.

Here, we introduce a general strategy for PADR by using DNA strand displacement (Fig. 1A). In a basic regulation module, a unique allosteric signal transduction mechanism was established where binding of an input leads to conformational changes and the concomitant release of an output, analogous to the action of a nutcracker (Fig. 1, B and C). As no direct contact occurs between I/O signals in PADR, the sequences of I/O DNA strands can be designed with complete orthogonality and high flexibility (Fig. 1D). We experimentally validated that the activity of PADR can be regulated by programmable conformational modulations. The designs of PADR networks are flexible and scalable, as confirmed by constructing fan-out/fan-in and multiple-layer cascading allosteric DNA networks. This strategy also enabled the construction of an allosteric origami nanomachine of 100 nm in size to perform a long-range conformational signal transmission.

RESULTS

Basic allosteric DNA regulation module

In implementing PADR, an ideal basic regulation module design should have essential characteristics such as sensitive conformational responsiveness, accurate allosteric tunability, programmable signal

[1]School of Computer Science, Key Lab of High Confidence Software Technologies, Peking University, Beijing 100871, China. [2]School of Control and Computer Engineering, North China Electric Power University, Beijing 102206, China. [3]Bio-evidence Sciences Academy, Xi'an Jiaotong University, Xi'an, Shaanxi 710049, China. [4]College of Computer Science, Shenyang Aerospace University, Shenyang 110136, China. [5]Wallace H. Coulter Department of Biomedical Engineering, Georgia Institute of Technology and Emory University, Emory University School of Medicine, Atlanta, GA 30322, USA. [6]Department of Chemistry, Emory University, Atlanta, GA 30322, USA. [7]Key Laboratory of Organic Optoelectronics and Molecular Engineering of the Ministry of Education, Department of Chemistry, Tsinghua University, Beijing 100084, China. [8]The State Key Laboratory of Bioelectronics, Southeast University, Nanjing 211189, China. [9]Center for Molecular Design and Biomimetics, The Biodesign Institute, Arizona State University, Tempe, AZ 85287, USA. [10]School of Molecular Sciences, Arizona State University, Tempe, AZ 85287, USA.
*Corresponding author. Email: zhangcheng369@pku.edu.cn (C.Z.); yjzcdd_2000@ncepu.edu.cn (J.Y.); hao.yan@asu.edu (H.Y.)
†These authors contributed equally to this work.

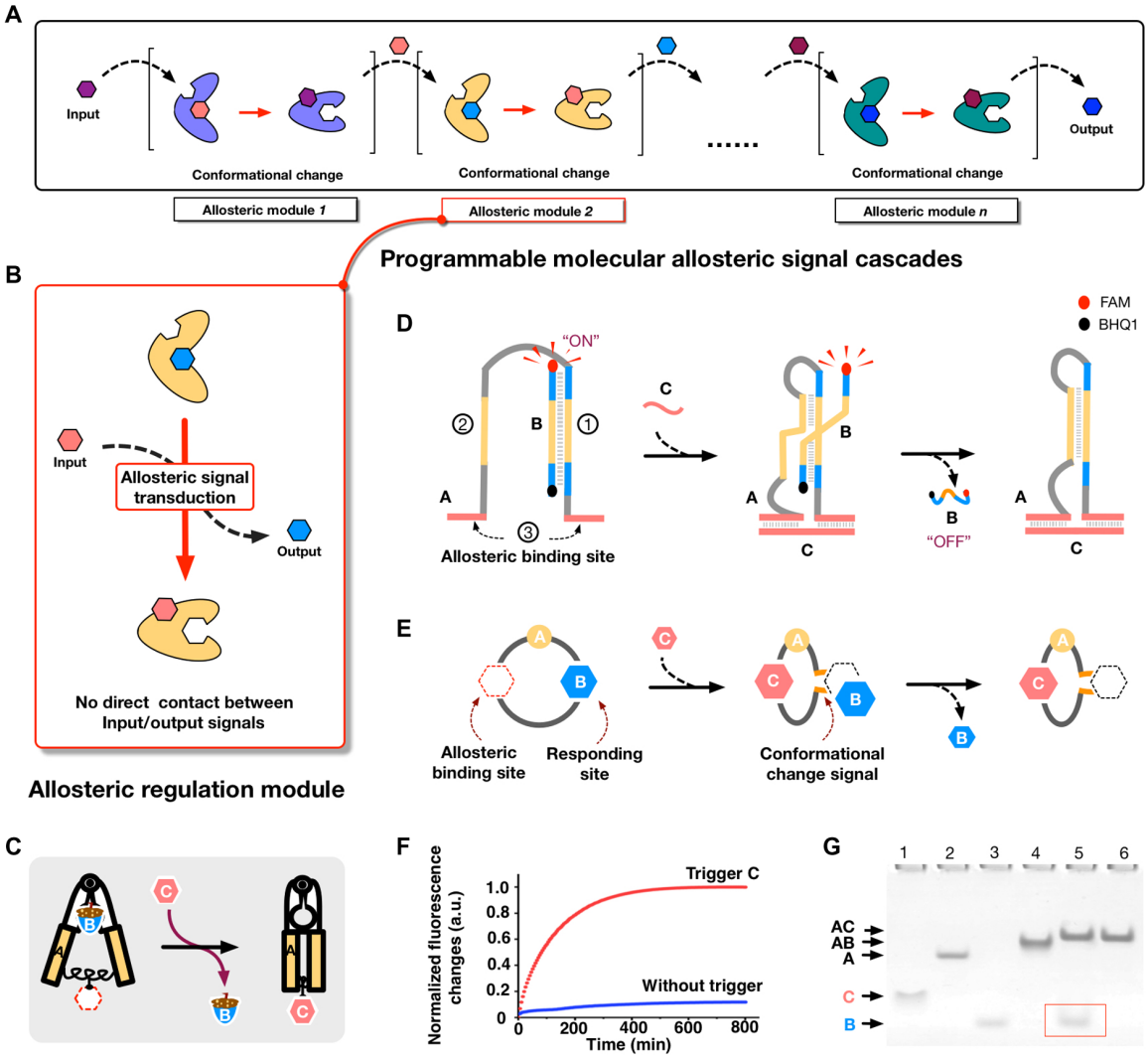

Fig. 1. Schematic illustrations of PADRs. (**A**) Allosteric cascades. (**B**) Basic allosteric regulation module. (**C**) Cartoon drawings of allosteric DNA regulation, which is similar to a nutcracker device. (**D**) The design details of allosteric DNA regulation. (**E**) Schematic diagrams of the allosteric DNA regulation module. (**F**) Fluorescence assay to monitor the module of PADR. [AB] = 0.5 μM and [C] = 0.5 μM. a.u., arbitrary units. (**G**) Analysis of basic allosteric regulation by PAGE. Lane 1, C; lane 2, A; lane 3, B; lane 4, AB; lane 5, A/B + C; lane 6, A/C.

integration, and multiple synergistic effects (Fig. 1A). Therefore, a unique chemical/conformational signal transduction mechanism was developed to implement basic allosteric regulations (Fig. 1, D and E). The binding of an input to the target receptor triggers a conformational change that causes the release of an output at a responding site (Fig. 1B).

In the design, DNA complex A/B serves as a receptor consisting of two DNA strands (i.e., A and B) that form a basic receptor for the allosteric module (Fig. 1D). DNA A has three functional domains: (1) an 18-nt binding domain that preferentially hybridizes with DNA B; (2) a 12-nt complementary domain that potentially hybridizes with the 18-nt binding domain to facilitate formation of an intramolecular hairpin structure by DNA A; and (3) allosteric binding sites, consisting of two separate 10-nt domains at the 3′ and 5′ ends of strand A, respectively.

In the initial state, DNA B preferentially hybridizes with DNA A, taking advantage of the two short extra hybridization domains (colored blue in Fig. 1D). Although complementary domain (2) can hybridize with domain (1), the designed thermodynamic state still favors hybridization of strands A and B (fig. S1). Therefore, the metastable hybridization state of complex A/B is susceptible to conformational changes. During allosteric regulation, input DNA C is designed to bind with the allosteric sites [domain (3)] to induce a conformational change (Fig. 1, D and E). Specifically, binding of DNA C pulls together the two ends of DNA A, leading to a juxtaposition of domains (1) and (2). This conformational change greatly increases the local concentrations of domains (1) and (2), which facilitates internal strand displacement and release of DNA B as an output while leaving DNA A as the internal hybridizing hairpin.

The results of the basic PADR operations were initially confirmed by fluorescence arrays (Fig. 1F). Release of single-stranded B, which adopts a random coil configuration in the unbound state, greatly reduces the distance between the fluorophore and quencher, thus leading to an efficient quenching effect. Accordingly, a significant

change in the fluorescent signal was observed by adding trigger C to complex A/B. (The simulation results of different trigger concentrations are presented in fig. S28). In native polyacrylamide gel electrophoresis (PAGE) analysis, upon introducing trigger C, a gel band corresponding to released DNA B was observed, and the gel band representing complex A/B disappeared concomitantly; thus, confirming the successful operation of the basic PADR module (Fig. 1G, lane 5). (More optimization experimental results are provided in figs. S6 and S7.)

Conformational fine-tuning of allosteric DNA regulation

In protein allosteric modulations, conformational signals can be tuned to regulate cellular responses (*12*–*14*). Similarly, the basic PADR can be fine-tuned by adjusting the input-binding–induced conformational signals to output-defined concentrations of target DNA. Here, fine-tuning the allosteric signal was realized by introducing a regulator T1 (poly-T spacer) in the middle of trigger C (Fig. 2A). During regulation, the regulator can be adjusted from a relaxed state to a coiled state by varying the length of T1, thus precisely controlling the distances between domains (1) and (2). That means trigger C–induced allosteric signals can regulate the local concentrations of domains (1) and (2), to finely control over the release of DNA B.

This fine-tuning of the allosteric response was verified by PAGE analysis and a fluorescence array. Eighteen different triggers were used as DNA inputs with spacer lengths ranging between 0 and 63 nt (Fig. 2B). The PAGE results demonstrated that the release of DNA B gradually decreased as the spacer length increased. Moreover, no gel band of complex A/B was observed following the introduction of DNA C. The gel results indicate that tunable allosteric regulation is feasible. In addition, fluorescence assays were used to investigate this allosteric regulation (Fig. 2C). The fluorescence intensity was observed to decrease as the spacer length increased. In particular, conformation-modulating triggers with spacer lengths ranging from 0 to 21 nt performed most effectively, as the length variations increased the rate constants considerably from 3.45×10^2 to 2.07×10^1 liter/mol·s, respectively (fig. S29). The simulation results of the bottom spacer regulations are presented in fig. S29.

Conformational specificity guarantees "structural no-target safety" in protein allosteric signal regulations, even under high reactant stoichiometric ratios (*13*). Input DNAs C2, C10, and C21 (with spacer lengths of 2, 10, and 21 nt, respectively) were selectively examined to verify that such conformational specificity also exists in allosteric DNA regulation, with trigger to receptor concentration ratios ranging from 0.25 to 2.0 (Fig. 2D). The results showed that increasing the trigger concentrations failed to produce a change in fluorescence

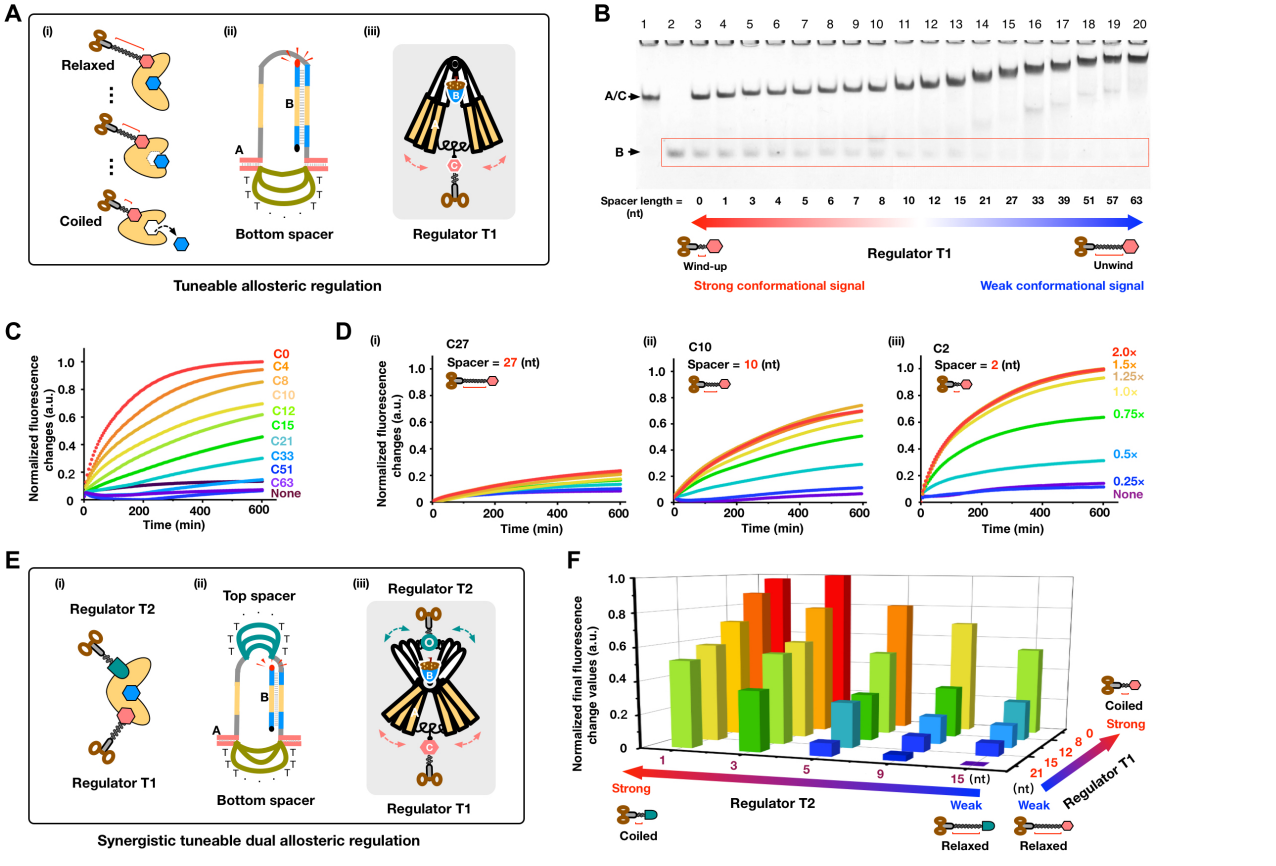

Fig. 2. Conformational fine tuning of allosteric regulation. (**A**) Schematic illustration showing how conformational changes are fine-tuned by adjusting the length of regulator T1. (**B**) PAGE gel results of modulated allosteric regulation with spacer lengths varying from 0 to 63 nt. (**C**) Fluorescence assay monitoring conformational modulations with varying lengths of T1. (**D**) Fluorescence assay using varying concentrations (from 0.125 to 1 μM) of DNA triggers C2, C10, and C27 with T1 lengths of 2, 10, and 27 nt, respectively. (**E**) Schematic illustration of synergistic dual fine-tuning of allosteric regulation by adjusting the lengths of regulators T1 and T2 simultaneously. (**F**) Histograms of the fluorescence data for synergistic dual allosteric regulation (fluorescence intensities at a reaction time of 600 min).

when C27 was used as the input. This result indicates that conformational signal modulation was too weak to cause effective allosteric regulation. In contrast, input C2 with a shorter spacer yielded a much larger distribution of signals. Thus, input DNA with a given spacer length was demonstrated to finely control conformational signal modulation, thereby guaranteeing structural no-target safety in the fine adjustment of allosteric signals.

We then attempted to synergistically and programmably regulate allostery by using multiregulators, which should be possible given the flexibility afforded with using DNA designs. Dual allosteric regulation was implemented by using two regulators T1 and T2 simultaneously (Fig. 2E). We also confirmed that the top regulator T2 modulates allosteric regulation (fig. S12). By simultaneously varying the lengths of both T1 and T2, 25 different synergetic allosteric regulations were generated (Fig. 2F). The largest increase in fluorescence intensity was achieved when T1 = 0 nt and T2 = 3 nt, whereas the lowest fluorescence intensity was observed when T1 = 21 nt and T2 = 15 nt. In addition, the results of the fluorescence variations are shown in fig. S15, where a series of sensitive synergistic regulations were implemented. The simulation results of the synergistic regulations are shown in figs. S30 and S31.

Allosteric DNA signal networks

Given that no predefined sequence is required between I/O DNA strands because of the orthogonality, various PADR pathways with programmable allosteric signal integrations can be implemented such as fan-out/fan-in operations and cascading networks.

Initially, a three-output fan-out allosteric DNA gate was constructed where all three DNA receptors (F1/D1, F2/D2, and F3/D3) were designed to respond to one input E with the release of three different outputs, D1, D2, and D3, respectively (Fig. 3A). Three types of DNA outputs were observed in gel results when DNA trigger E was added to the fan-out receptors (Fig. 3B, lane 2) (additional poly-T tails with different lengths were added to DNA outputs D1, D2, and D3 to improve the gel band discrimination, and more experimental results of the fan-out operations are provided in figs. S17 and S18). Meanwhile, the fan-out results were also monitored by the fluorescence array. The addition of input E gave three types of fluorescence variations, corresponding to the simultaneous observation of FAM (carboxyfluorescein), HEX (hexachloro fluorescein), and carboxy-X-rhodamine (Fig. 3C). In addition, a three-input fan-in allosteric DNA gate was also constructed on the basis of the allosteric regulation strategy, where one DNA output B can be triggered by any of the three different DNA inputs (Fig. 3, D to F, and fig. S20).

Next, a four-layer PADR cascading network was constructed to investigate the programmable integration of allosteric signals. Hierarchical designs were used to pass conformational signals from the upstream unit to its neighboring downstream unit (Fig. 3G). Upon introducing the initial input E in layer 1, the first DNA receptor F1/D1 was triggered to release DNA D1, which targets the allosteric

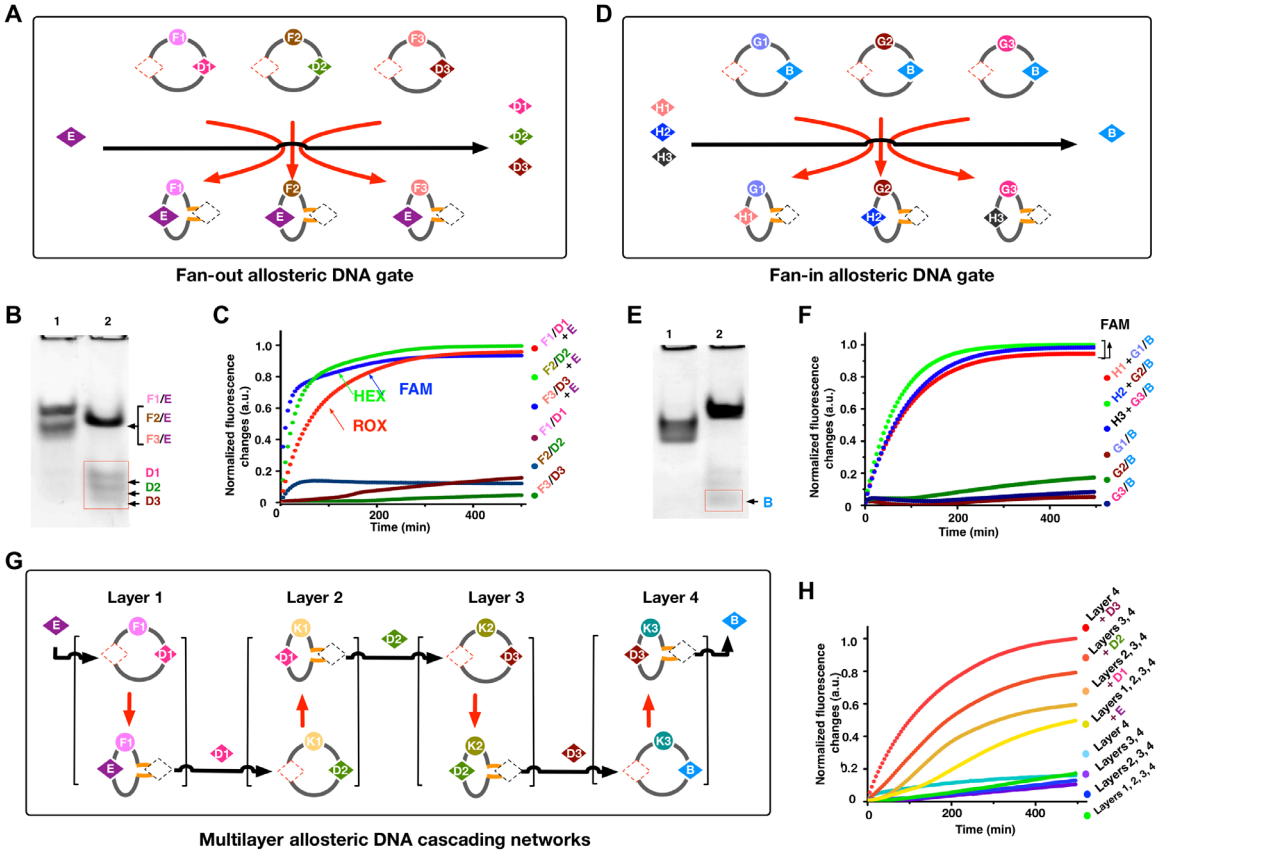

Fig. 3. Allosteric DNA signal networks. (**A**) Schematic illustration of the fan-out allosteric DNA gate. (**B**) Analysis of the fan-out gate by PAGE. Lane 1, without trigger; lane 2, with trigger E. (**C**) Results of the fluorescence assay for the fan-in allosteric DNA gate. (**D**) Schematic illustration of the fan-in allosteric DNA gate. (**E**) PAGE analysis of the fan-in DNA gate with simultaneous triggering by H1, H2, and H3. Lane 1, without input; lane 2: with inputs H1, H2, and H3, simultaneously. (**F**) Fluorescence assay of the fan-in allosteric DNA gate. (**G**) Schematic illustration of four-layer allosteric DNA cascading networks. (**H**) Analysis of the cascading DNA networks by the fluorescence assay.

binding site of receptor K1/D2 (layer 2). The continuous cascading allosteric regulation events resulted in the gradual activations of DNA receptors K2/D3 (layer 3) and K3/B (layer 4). Last, output B was released from the last receptor K3/B in layer 4. In the PAGE gel results in fig. S23 (lane 9), after being triggered by initial input E, a new gel band representing output B was obtained in the four-layer cascade network, confirming an effective allosteric signal integration and transmission cascade. In addition, the generation of a significant change in fluorescence also confirmed the allosteric signaling cascade of the four-layer PADR network (Fig. 3H). Increasing the number of cascading layers from 1 to 4 caused a gradual reduction in the change in the fluorescence signal. For example, when the number of cascading layers was increased from 1 to 2, the normalized final fluorescence yields were estimated to be below 80%. The gradual reduction in fluorescence yields suggests attenuation of the cascading signal transductions within the multilayer connections. (More experimental results related to the four-layer network are provided in figs. S22 to S27, and the related simulation results are shown in fig. S32).

A long-range allosteric DNA origami nanomachine

To explore the possibility that conformational signals can transmit remotely through rigid DNA origami structures, an origami nanomachine of 100 nm in size was established to implement a long-range PADR (L-PADR). In the long-range design, the first conformational signal-1 was mechanically transmitted across the origami structure to induce the second conformational signal-2, thus achieving long-range regulation at a responding site (Fig. 4A). Specifically, the nanomachine consisted of two sections: DNA origami O and DNA/AuNP receptor H/G (Fig. 4B). The "Y" shape origami O had two dynamic swing arms and one handle. The allosteric binding sites A.1 and A.2 were designed at the end of the origami arms. Accordingly, DNA L was designed to bind with sites A.1 and A.2 to control the "open/close" state of the two origami arms. In addition, two hybridization sites C.1 and C.2 were designed on the outside face of the origami arms to connect with receptor H/G. Here, receptor H/G was designed with two subunits: DNA H and DNA/AuNP conjugate G (with a 15-nm AuNP monovalently modified at the 3′ end of thiolated DNA G).

In the reaction, input DNA L initially binds at the allosteric sites A.1 and A.2 to induce conformational signal-1 by shifting the origami arms from the opened to closed state [Fig. 4B(i) and fig. S42]. Signal-1 can then be mechanically transmitted from the origami structure to receptor H/G by indirectly pulling together the two ends of DNA H. Such a conformational change serves as conformational signal-2, which subsequently leads to the release of DNA/AuNP G [Fig. 4B(ii)].

L-PADR was first verified by using an agarose gel method (Fig. 4C and fig. S46). A product gel band representing DNA origami binding with AuNP was observed under white light, as shown in Fig. 4C (lane 1), indicating the desired generation of the nanomachine.

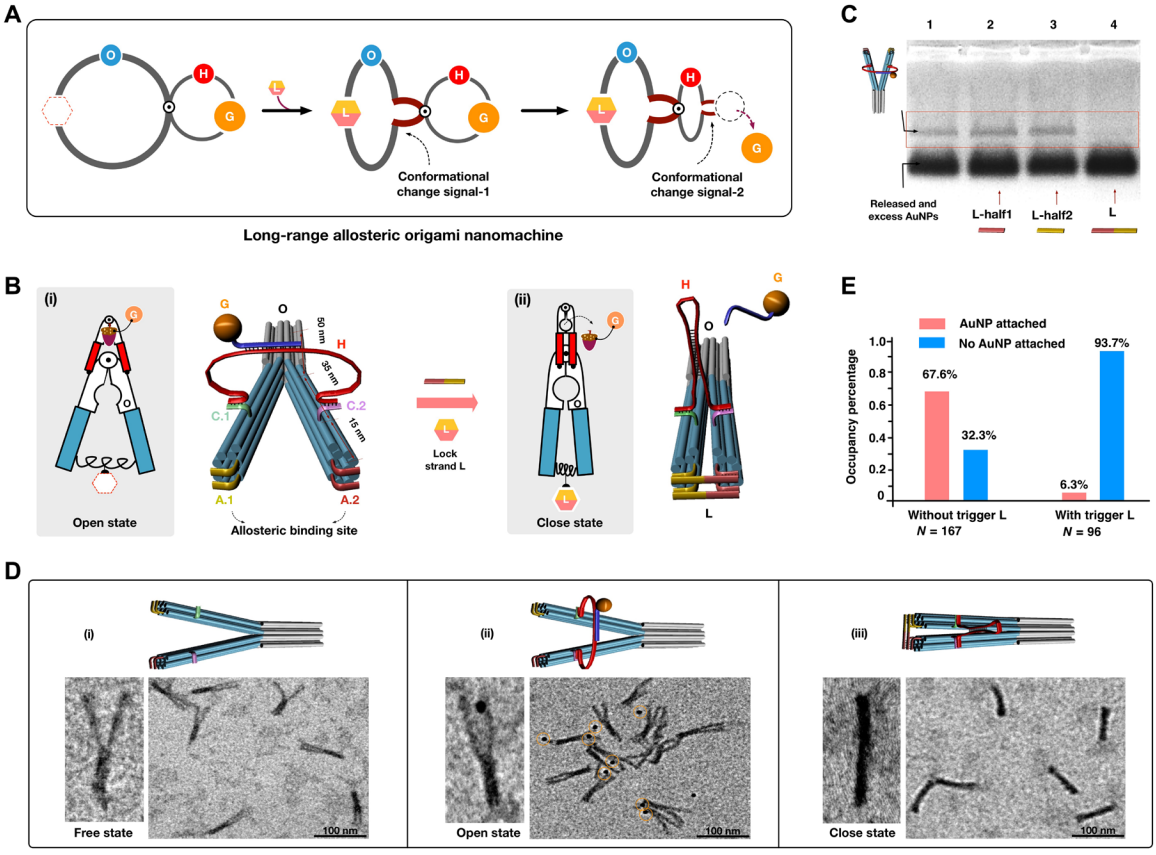

Fig. 4. Long-range allosteric DNA regulation using origami nanomachine. Schematic illustration (**A**) and cartoon drawings (**B**) of the designed origami structures with open and closed states of the arms, which are regulated by binding input DNA L. (**C**) Agarose gel analysis of L-PADR (1% gel, under white light). (**D**) TEM images of the origami nanomachines with different conformational structures. (**E**) Statistical results of the AuNP occupancies before and after long-range allosteric regulation.

However, upon treatment with input DNA L, the target gel band corresponding to the nanoparticle binding nanomachine disappeared (lane 4). This result demonstrated that the 15-nm AuNP from the origami structure was released when treated with DNA L. To verify that the release of the AuNP was induced by allosteric regulation, incomplete DNA lock strands L1 and L2 (the left and right halves of the sequences of L) were used to trigger the nanomachine (Fig. 4C, lanes 2 and 3). Under these conditions, however, the intact gel bands corresponding to the initial nanomachine still appeared, thus indicating almost no release of AuNP from the origami. In addition, origami nanomachines with selective removal of allosteric sites on the origami arm were unable to induce AuNP release (fig. S45). Nonetheless, the absence of binding sites on either the lock strand or origami inhibited L-PADR. These results showed that long-range regulation controlled the release of AuNP from the origami.

To analyze the L-PADR effect on the origami nanomachine, transmission electron microscopy (TEM) images of three types of origami structures were collected: (i) free-state nanomachine, (ii) open-state nanomachine attached with one 15-nm AuNP, and (iii) closed-state nanomachine triggered by DNA L (Fig. 4D). The TEM results of the free-state structure (i) revealed that the two swing arms were predominantly in the open state and separated from each other. The images of structure (ii) showed that the two arms were primarily in the open state, and in most cases, one 15-nm AuNP occupied one origami structure. The origami structure remained primarily in the closed state when locked with DNA L [Fig. 4D(iii)], and almost no AuNP was attached to the origami structures. The statistical results of the nanoparticle occupancies also indicated that most of the nanomachines released DNA/AuNP conjugate G after long-range allosteric regulation (Fig. 4E and figs. S52 and S53).

Conformational fine-tuning of the long-range allosteric origami nanomachine

Because allosteric regulation can be finely tuned by adjusting the trigger spacer length, a similar strategy was adopted to fine-tune the L-PADR origami nanomachine (Fig. 5, A and B). By considering the much larger size of the origami structure, the lengths of the poly-T spacers in the middle of the input DNA L1 were chosen as 0, 20, 40, 60, and 99 nt (Fig. 5C). Thus, the states of the origami arms were precisely controlled to produce different types of conformational signal-1 (fig. S57). As the different inputs induced specific conformational signal-1, the receptor H/G produced various corresponding conformational signal-2, leading to the specific and precise regulated release of DNA/AuNP G. The long-range fine-tuning effects were confirmed by agarose gel analysis (Fig. 5D and fig. S46). The release of AuNP was observed to decrease gradually as the trigger loop length increased from 0 to 99 nt, indicating that the origami nanomachine can also be finely tuned using long-range allosteric signals.

In addition, the specificity of the conformational signals in long-range allosteric regulation was analyzed by varying the concentration of the input DNA trigger (Fig. 5E). The concentrations of DNA inputs L0 and L99 (with spacer lengths of 0 and 99 nt, respectively) were varied. The release of AuNPs was dependent on the concentrations of L0 as the input, with the amount of AuNP released gradually increasing as the concentration of L0 increased (Fig. 5E and figs. S47 and S48). In contrast, no such concentration-dependent effect was observed when using trigger L99. For example, when the concentrations of DNA input L0 and L99 increased to a ratio of trigger to origami of 10:1, the estimated decreases in AuNP release were below 10 and 80%, respectively. The specificity of the allosteric signal was demonstrated to even exist in the DNA origami with a much larger size of 100 nm, thus guaranteeing structural no-target safety in the allosteric origami nanomachine.

DISCUSSION

In this report, we have demonstrated a general strategy of allosteric DNA regulation to construct synthetic molecular networks and origami nanomachines. Cascading allosteric DNA networks were established by organizing individual allosteric modules in a programmable manner

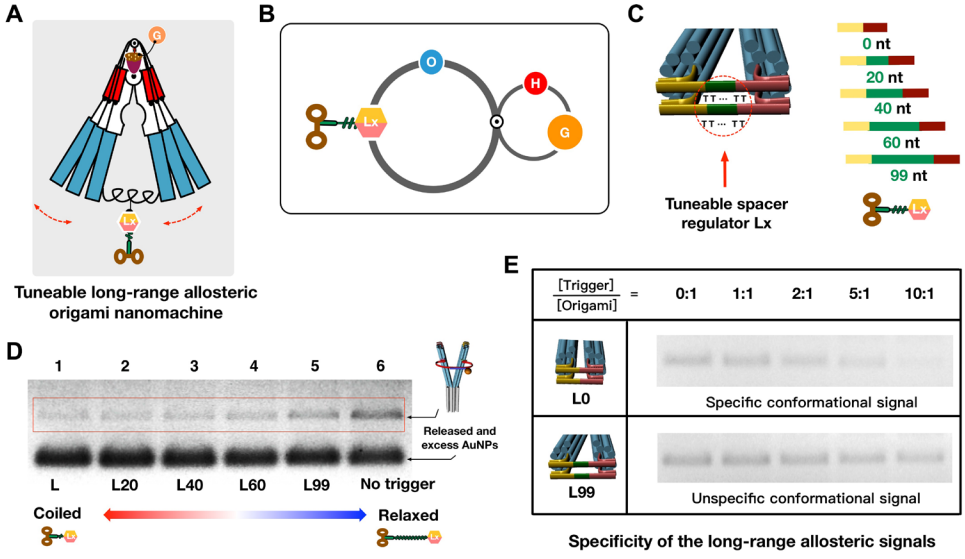

Fig. 5. Finely tuned long-range allosteric regulation. A cartoon drawing (**A**) and schematic illustration (**B**) of the allosteric regulation on an origami nanomachine by adjusting the trigger spacer lengths in lock DNA Lx (**C**). (**D**) Agarose gel (1%) analysis of the long-range allosteric nanomachine under different allosteric regulation, i.e., different lengths of DNA Lx. (**E**) Comparison of allosteric signal specificities when using L0 and L99 during the long-range allosteric regulation (all gel results were detected under white light).

because signal transduction and integration can be uniformly determined in each module. In addition, the PADR scheme can be finely tuned by varying conformational signals with different spatial dimensions, positions, and number of regulators. We have constructed a series of allosteric DNA systems: the fan-out/fan-in gates and a four-layer cascading network and a long-range allosteric origami nanomachine.

Compared with these strategies, the modular, integrative, and synergistic design properties of PADR make this strategy particularly suitable for engineering allosteric DNA pathways in a programmable manner. The strategy provides a modularized tool to construct programmable allosteric signal networks. Fewer predefined sequence constraints are required because direct contact between I/O DNA strands is avoided, thus facilitating the organization of individual allosteric modules into networks. The allosteric strategy also endows the DNA regulations by fine-tuning conformational signals. In this study, the programmable fine-tuning of the conformation was demonstrated by changing the dimensions, positions, and number of conformational signals, where even dual-conformational regulation was shown to control reactions synergistically. In addition, allosteric regulation was implemented on the origami nanomachines, where long-range allosteric signals were transmitted through the 50-nm-long origami arms. Such long-range allosteric signals can even be tuned remotely by changing the origami conformations at the nanoscale level.

In cells, responding to allosteric ligand binding, riboswitch usually adopts dynamic conformational change or various folding structures to affect its catalytic ability for regulating gene expressions. Similar to the conformational signals used to engineer biofunctions in nature, any biomolecule or external physical stimulation that induces subtle conformational changes can also potentially serve as an allosteric signal to trigger the programmable allosteric DNA networks, subsequently inducing downstream reactions. In reality, many artificial allosteric DNA networks have already provided exciting opportunities for catalysis regulation (*51*) and catalytic signal processing (*52*–*54*), which will have more applications in biomedicine and molecular sensing. We expect that these allosteric systems will enhance the potential scope of biological applications for the PADR strategy greatly.

Different from other reported allosteric DNA operations (e.g., DNA receptors, probes, and beacons) (*47*–*49*) and regulation mechanisms (e.g., aptamer initiation, pH control, and enzyme assistance), the reported strategy is a general and programmable DNA regulation method based on DNA strand displacement. This method should enable the building of complex, large-scale, and cascade allosteric DNA networks in a programmable way. Therefore, we envision that this strategy will enable the development of a series of programmable allosteric signals that mediate biomolecular systems and nanodevices for various biomedical and nanoengineering applications.

MATERIALS AND METHODS

Reagents and materials

All oligonucleotides (table S1) were obtained from Sangon Company (China). The thoilated and fluorophore modified DNA molecules were purified with high-performance liquid chromatography. The DNA sequence designs were analyzed using NUPACK (http://nupack.org) to ensure that minimal cross-talk existed between undesirable domains. During the experiments, for convenience, all DNA strands were stored in 20 to 100 μM stocks in ultrapure H_2O at −20°C. During the experiment, the DNA concentrations were carefully quantified by absorbance measurements at 260 nm using a Nanodrop or ultraviolet (UV) spectrophotometer (PERSEE, 1901). Then, the DNA concentrations were calculated by using extinction coefficients that had been provided by Sangon Company. Fifteen-nanometer gold nanoparticles were obtained from Ted Pella.

Fluorescence assay

All experiments were performed at 25°C in a 1× tris-acetate-EDTA (TAE)/Mg^{2+} buffer using a real-time fluorescence polymerase chain reaction (Agilent Technologies). Here, the time dependence of the fluorescence signal was normalized to make the initial value starts at zero. The detection time interval was 2 to 5 min. The fluorescence results were obtained by averaging the values from three replicates of the experimental results.

PAGE experiments

The reactions of the allosteric regulation were verified using native PAGE. During the experiments, a 12% gel was made with 1× TAE/Mg^{2+} buffer that had been supplemented with 12.5 mM $MgCl_2$. All samples were run at 100 V for 1.5 to 2 hours at 4°C. After staining the polyacrylamide gels with Stain-All, the gels were then imaged by a scanner (Canon LIDE 100). To detect the FAM fluorophores and the HEX-modified DNA complexes, the gels were imaged under UV light without staining, using a Fluorchem FC2 gel scanner or camera.

Calculations of the fluorescence results

To make the fluorescence results easy to understand, the original fluorescence results of the reaction are calculated by a standard normalization date process method. After the calculations, the decreased fluorescence results are translated into the calculated results with increasing variation values, where the information of signal relative variation is well kept in the calculated results (fig. S4C). Therefore, all fluorescence result variation ranges between [0, 1] sections. The fluorescence results are calculated on the basis of the normalized method using the following equation

$$\text{Normalized fluorecence change ratio} = \frac{F_i - F_R}{F_i}$$

F_i represents the fluorescence intensity without DNA C triggering, as obtained from the reactions: 0.5 μM reactant A/B DNA complex in TAE/Mg^{2+} buffer. The F_R is the fluorescence intensity triggered with DNA C.

Simulations of the kinetics of the reactions

In this study, a general representation, explicit state-space form (*55*), was used to model the processes of the allosteric DNA regulation reactions mathematically. In this uniform representation schema, the dynamic reactions were represented by a set of input, output, and state variables related by first-order differential equations. Moreover, the state variables defined the values of the output variables. During the simulation, at first, all reaction formulas were mathematically modeled on the basis of the explicit state-space forms. Then, experimental data were used to estimate the unknown parameters in the mathematical model by using a nonlinear gray-box model (*56*). Last, the whole reaction process was simulated by using the updated parameters based on the well-established mathematical model. According to the specific modifications in this study, the changes of

fluorescent value were calculated through the initial fluorescent value minus the current fluorescent value. Given that the product concentration is directly proportional to the fluorescence intensity, the output of the dynamic reaction system can be measured by the changes of fluorescent value, as mentioned above. More simulation details are provided in figs. S28 to S32.

Preparations of the long-range allosteric origami nanomachine

For Y shape DNA clamp origami assembly, the staple DNA strands were mixed at equal molar ratios (15 nM) with M13mp18 strand in TAE/Mg^{2+} buffer. The mixture was subjected to an annealing procedure for over 16 hours. Then, hairpin DNA H was introduced to the prepared DNA origami nanostructures, using the following thermal annealing from 40° to 25°C. After assembly, the origami products were purified using a 100-kDa molecular weight cutoff (MWCO) Microcon centrifugal filter (Amicon). To prepare the monovalent DNA/AuNP complex G, the ratios of DNA with AuNPs were selectively controlled. The thiolated DNA strand was incubated with 15-nm AuNPs at the concentration ratio of 1:2, in 0.5× TBE buffer [89 mM tris, 89 mM boric acid, and 2 mM EDTA (pH 8.0)] and a final NaCl concentration of 50 mM for 4 to 6 hours at room temperature. After conjugation, 3% agarose gel was used to separate monovalent AuNP/DNA conjugates (running gel buffer, 0.5× TBE, 70 V, 1.5 hours).

Then, the purified monovalent 15-nm DNA/AuNP conjugate was introduced to hybridize with the initial DNA origami, in a large excess concentration ratio (200:1), at room temperature for 6 hours. Last, the products can be detected by using 1% agarose gels (0.5× TBE and 5.5 mM Mg^{2+} running buffer) for 1.5 to 2.5 hours. The target origami nanomachine was collected from the gel for TEM imaging by a glass fiber filter membrane supported by a dialysis membrane (MWCO, 14000).

Long-range allosteric regulation using DNA origami nanomachine

The long-range allosteric origami nanomachine can be regulated by introducing DNA input L to release the target DNA/AuNP complex. Specifically, the AuNP/origami nanomachine was mixed with an excess of lock DNA L (ratio = 1:10) at room temperature for 6 to 8 hours. Then, the reaction results were monitored by 1% agarose gel at 55 V for 1.5 to 2.5 hours (0.5× TBE and 5.5 mM Mg^{2+} running buffer). The gel images were obtained by using a gel imaging system (Tanon 2500).

SUPPLEMENTARY MATERIALS

Supplementary material for this article is available at https://science.org/doi/10.1126/sciadv.abl4589

REFERENCES AND NOTES

1. B. Kholodenko, M. B. Yaffe, W. Kolch, Computational approaches for analyzing information flow in biological networks. *Sci. Signal.* **5**, 2002961 (2012).
2. J. Hitomi, D. E. Christofferson, A. Ng, J. Yao, A. Degterev, R. J. Xavier, J. Yuan, Identification of a molecular signaling network that regulates a cellular necrotic cell death pathway. *Cell* **135**, 1311–1323 (2008).
3. B. D. Manning, A. Toker, AKT/PKB signaling: Navigating the network. *Cell* **169**, 381–405 (2017).
4. A. Vinayagam, U. Stelzl, R. Foulle, S. Plassmann, M. Zenkner, J. Timm, H. E. Assmus, M. A. Andrade-Navarro, E. E. Wanker, A directed protein interaction network for investigating intracellular signal transduction. *Sci. Signal.* **4**, rs8 (2011).
5. B. Deplancke, A. Mukhopadhyay, W. Ao, A. M. Elewa, C. A. Grove, N. J. Martinez, R. Sequerra, L. Doucette-Stamm, J. S. Reece-Hoyes, I. A. Hope, H. A. Tissenbaum, S. E. Mango, A. J. M. Walhout, A gene-centered *C. elegans* protein-DNA interaction network. *Cell* **125**, 1193–1205 (2006).
6. E. Buck, R. Iyengar, Organization and functions of interacting domains for signaling by protein-protein interactions. *Sci. STKE* **2003**, re14 (2003).
7. P. J. Conn, A. Christopoulos, C. W. Lindsley, Allosteric modulators of GPCRs: A novel approach for the treatment of CNS disorders. *Nat. Rev. Drug Discov.* **8**, 41–54 (2009).
8. A. P. Kornev, S. S. Taylor, Dynamics-driven allostery in protein kinases. *Trends Biochem. Sci.* **40**, 628–647 (2015).
9. O. Dagliyan, N. V. Dokholyan, K. M. Hahn, Engineering proteins for allosteric control by light or ligands. *Nat. Protoc.* **14**, 1863–1883 (2019).
10. Z. H. Foda, Y. Shan, E. T. Kim, D. E. Shaw, M. A. Seeliger, A dynamically coupled allosteric network underlies binding cooperativity in Src kinase. *Nat. Commun.* **6**, 5939 (2015).
11. J. D. Schwartz, X. Zhang, S. G. Nathenson, S. C. Almo, Structural mechanisms of costimulation. *Nat. Immunol.* **3**, 427–434 (2002).
12. D. M. Thal, A. Glukhova, P. M. Sexton, A. Christopoulos, Structural insights into G-protein-coupled receptor allostery. *Nature* **559**, 45–53 (2018).
13. F. D. Smet, A. Christopoulos, P. Carmeliet, Allosteric targeting of receptor tyrosine kinases. *Nat. Biotechnol.* **32**, 1113–1120 (2014).
14. J. Changeux, 50 years of allosteric interactions: The twists and turns of the models. *Nat. Rev. Mol. Cell Biol.* **14**, 819–829 (2013).
15. G. Gourinchas, S. Etzl, C. Gobl, U. Vide, T. Madl, A. Winkler, Long-range allosteric signaling in red light-regulated diguanylyl cyclases. *Sci. Adv.* **3**, e1602498 (2017).
16. J. Changeux, S. J. Edelstein, Allosteric mechanisms of signal transduction. *Science* **308**, 1424–1428 (2005).
17. R. Wei, X. Wang, Y. Zhang, S. Mukherjee, L. Zhang, Q. Chen, X. Huang, S. Jing, C. Liu, S. Li, G. Wang, Y. Xu, S. Zhu, A. J. Williams, F. Sun, C. Yin, Structural insights into Ca^{2+}-activated long-range allosteric channel gating of RyR1. *Cell Res.* **26**, 977–994 (2016).
18. S. Isogai, X. Deupi, C. Opitz, F. M. Heydenreich, C. J. Tsai, F. Brueckner, G. F. X. Schertler, D. B. Veprintsev, S. Grzesiek, Backbone NMR reveals allosteric signal transduction networks in the β1-adrenergic receptor. *Nature* **530**, 237–241 (2016).
19. A. A. Green, J. Kim, D. Ma, P. A. Silver, J. J. Collins, P. Yin, Complex cellular logic computation using ribocomputing devices. *Nature* **548**, 117–121 (2017).
20. X. J. Gao, L. S. Chong, M. S. Kim, M. B. Elowitz, Programmable protein circuits in living cells. *Science* **361**, 1252–1258 (2018).
21. R. Gaber, T. Lebar, A. Majerle, B. Ster, A. Dobnikar, M. Bencina, R. Jerala, Designable DNA-binding domains enable construction of logic circuits in mammalian cells. *Nat. Chem. Biol.* **10**, 203–208 (2014).
22. C. J. Delebecque, P. A. Silver, A. B. Lindner, Designing and using RNA scaffolds to assemble proteins in vivo. *Nat. Protoc.* **7**, 1797–1807 (2012).
23. T. Kitada, B. Diandreth, B. Teague, R. Weiss, Programming gene and engineered-cell therapies with synthetic biology. *Science* **359**, eaad1067 (2018).
24. P. Yin, H. M. T. Choi, C. R. Calvert, N. A. Pierce, Programming biomolecular self-assembly pathways. *Nature* **451**, 318–322 (2008).
25. A. J. Genot, J. Bath, A. J. Turberfield, Reversible logic circuits made of DNA. *J. Am. Chem. Soc.* **133**, 20080–20083 (2011).
26. D. Y. Zhang, A. J. Turberfield, B. Yurke, E. Winfree, Engineering entropy-driven reactions and networks catalyzed by DNA. *Science* **318**, 1121–1125 (2007).
27. A. J. Thubagere, W. Li, R. F. Johnson, Z. Chen, S. Doroudi, Y. L. Lee, G. Izatt, S. Wittman, N. Srinivas, D. Woods, E. Winfree, L. Qian, A cargo-sorting DNA robot. *Science* **357**, 1112–1112 (2017).
28. W. Lai, L. Ren, Q. Tang, X. Qu, J. Li, L. Wang, L. Li, C. Fan, H. Pei, Programming chemical reaction networks using intramolecular conformational motions of DNA. *ACS Nano* **12**, 7093–7099 (2018).
29. G. Chatterjee, N. Dalchau, R. A. Muscat, A. Phillips, G. Seelig, A spatially localized architecture for fast and modular DNA computing. *Nat. Nanotechnol.* **12**, 920–927 (2017).
30. X. Yang, Y. Tang, S. M. Traynor, F. Li, Regulation of DNA strand displacement using an allosteric DNA toehold. *J. Am. Chem. Soc.* **138**, 14076–14082 (2016).
31. A. Amodio, E. D. Grosso, A. Troina, E. Placidi, F. Ricci, Remote electronic control of DNA-based reactions and nanostructure assembly. *Nano Lett.* **18**, 2918–2923 (2018).
32. Y. Xing, Z. Yang, D. Liu, A responsive hidden toehold to enable controllable DNA strand displacement reactions. *Angew. Chem. Int. Ed. Eng.* **50**, 11934–11936 (2011).
33. F. Huang, M. You, D. Han, X. Xiong, H. Liang, W. Tan, DNA branch migration reactions through photocontrollable toehold formation. *J. Am. Chem. Soc.* **135**, 7967–7973 (2013).
34. A. Amodio, B. Zhao, A. Porchetta, A. Idili, M. Castronovo, C. Fan, F. Ricci, Rational design of pH-controlled DNA strand displacement. *J. Am. Chem. Soc.* **136**, 16469–16472 (2014).
35. C. W. Brown III, M. R. Lakin, E. K. Horwitz, M. L. Fanning, H. E. West, D. Stefanovic, S. W. Graves, Signal propagation in multi-layer DNAzyme cascades using structured chimeric substrates. *Angew. Chem. Int. Ed. Eng.* **126**, 1–6 (2014).
36. M. Centola, J. Valero, M. Famulok, Allosteric control of oxidative catalysis by a DNA rotaxane nanostructure. *J. Am. Chem. Soc.* **139**, 16044–16047 (2017).

37. S. F. J. Wickham, J. Bath, Y. Katsuda, M. Endo, K. Hidaka, H. Sugiyama, A. J. Turberfield, A DNA-based molecular motor that can navigate a network of tracks. *Nat. Nanotechnol.* **7**, 169–173 (2012).
38. X. Chen, Expanding the rule set of DNA circuitry with associative toehold activation. *J. Am. Chem. Soc.* **134**, 263–271 (2012).
39. M. Weitz, J. Kim, K. Kapsner, E. Winfree, E. Franco, F. C. Simmel, Diversity in the dynamical behaviour of a compartmentalized programmable biochemical oscillator. *Nat. Chem.* **6**, 295–302 (2014).
40. D. Y. Zhang, G. Seelig, Dynamic DNA nanotechnology using strand-displacement reactions. *Nat. Chem.* **3**, 103–113 (2011).
41. N. E. C. Haley, T. E. Ouldridge, I. M. Ruiz, A. Geraldini, A. A. Louis, J. Bath, A. J. Turberfield, Design of hidden thermodynamic driving for non-equilibrium systems via mismatch elimination during DNA strand displacement. *Nat. Commun.* **11**, 2562 (2020).
42. S. W. Schaffter, R. Schulman, Building in vitro transcriptional regulatory networks by successively integrating multiple functional circuit modules. *Nat. Chem.* **11**, 829–838 (2019).
43. B. Wang, C. Thachuk, A. D. Ellington, E. Wingree, D. Soloveichik, Effective design principles for leakless strand displacement systems. *Proc. Natl. Acad. Sci. U.S.A.* **115**, E12182–E12191 (2018).
44. B. Chakraborty, R. Sha, N. C. Seeman, A DNA-based nanomechanical device with three robust states. *Proc. Natl. Acad. Sci. U.S.A.* **105**, 17245–17249 (2008).
45. J. L. Vinkenborg, N. Karnowski, M. Famulok, Aptamers for allosteric regulation. *Nat. Chem. Biol.* **7**, 519–527 (2011).
46. J. Song, Z. Li, P. Wang, T. Meyer, C. Mao, Y. Ke, Reconfiguration of DNA molecular arrays driven by information relay. *Science* **357**, eaan3377 (2017).
47. E. D. Grosso, G. Ragazzon, L. J. Prins, F. Ricci, Fuel-responsive allosteric DNA-based aptamers for the transient release of ATP and cocaine. *Angew. Chem. Int. Ed.* **58**, 5582–5586 (2019).
48. F. Ricci, A. Vallee-Belisle, A. Porchetta, K. W. Plaxco, Rational design of allosteric inhibitors and activators using the population-shift model: In vitro validation and application to an artificial biosensor. *J. Am. Chem. Soc.* **134**, 15177–15180 (2012).
49. S. Ranallo, C. Prévost-Tremblay, A. Idili, A. Vallée-Bélisle, F. Ricci, Antibody-powered nucleic acid release using a DNA-based nanomachine. *Nat. Commun.* **8**, 15150 (2017).
50. A. Porchetta, A. Vallee-Belisle, K. W. Plaxco, F. Ricci, Allosterically tunable, DNA-based switches triggered by heavy metals. *J. Am. Chem. Soc.* **135**, 13238–13241 (2013).
51. C. Wang, L. Yue, I. Willner, Controlling biocatalytic cascades with enzyme-DNA dynamic networks. *Nat. Catal.* **3**, 941–950 (2020).
52. L. Yue, S. Wang, V. Wulf, S. Lilienthal, F. Remacle, R. D. Levine, I. Willner, Consecutive feedback-driven constitutional dynamic networks. *Proc. Natl. Acad. Sci. U.S.A.* **116**, 2843–2848 (2019).
53. Z. X. Zhou, L. Yue, S. Wang, J. M. Lehn, I. Willner, DNA-based multiconstituent dynamic networks: Hierarchical adaptive control over the composition and cooperative catalytic functions of the systems. *J. Am. Chem. Soc.* **140**, 12077–12089 (2018).
54. Z. X. Zhou, O. Y. Yu, J. B. Wang, I. Willner, Dissipative gated and cascaded DNA networks. *J. Am. Chem. Soc.* **143**, 5071–5079 (2021).
55. S. N. Norman, *Control Systems Engineering* (Wiley, ed. 7, 2014).
56. T. P. Bohlin, *Practical Grey-box Process Identification: Theory and Applications* (Springer, 2006).
57. A. J. Genot, D. Y. Zhang, J. Bath, A. J. Turberfield, Remote Toehold: A Mechanism for flexible control of DNA hybridization kinetics. *J. Am. Chem. Soc.* **133**, 2177–2182 (2011).
58. K. Suzuki, K. Hosokawa, M. Maeda, Controlling the number and positions of oligonucleotides on gold nanoparticle surfaces. *J. Am. Chem. Soc.* **131**, 7518–7519 (2009).
59. D. Zanchet, C. M. Micheel, W. J. Parak, D. Gerion, A. P. Alivisatos, Electrophoretic isolation of discrete Au nanocrystal/DNA conjugates. *Nano Lett.* **1**, 32–35 (2001).

Acknowledgments: We thank V. Pan and L. Bianji, Edanz Editing China, for editing the English text of a draft of this manuscript. **Funding:** This work was supported by the national key R&D Program of China (2017YFE0130600 and 2021YFF1200103), National Natural Science Foundation of China (61872007, 62073133, and 61972266), Beijing Natural Science Foundation (Z201100008320002), CAS Interdisciplinary Innovation Team (JCTD-2020-04), and grants from U.S. National Science Foundation to Y.K. and from the Arizona State University to H.Y.
Author contributions: C.Z. initiated the project and designed the experiments; J.Y., X.M., and K.C. designed the used DNA structures and performed the experiments. X.Z., J.Y., and C.Z. analyzed the data and performed the simulations. C.Z., J.Y., Y.K., and H.Y. wrote the paper. C.Z., J.Y., Z.L., and H.Y. supervised the project. C.Z., J.Y, X.M., X.Z., Z.L., D.L., Y.K., and H.Y. discussed the designs and results of the experiments. All authors commented on the manuscript. **Competing interests:** The authors declare that they have no competing interests. **Data and materials availability:** All data needed to evaluate the conclusions in the paper are present in the paper and/or the Supplementary Materials.

Submitted 15 July 2021
Accepted 9 December 2021
Published 2 February 2022
10.1126/sciadv.abl4589